Key Points:
- Preconditioning of the ionosphere plays a role in which mode of transport the magnetosphere enters
- No DP1 current system was found during the initiating substorm of steady magnetospheric convection event (SMC)
- The Hall conductance is much stronger during the initiating substorm of the SMC and throughout the SMC compared to the isolated substorm

Comparison of the Ionosphere During an SMC Initiating Substorm and an Isolated Substorm

A. D. DeJong[1] [ID] **, J. M. Bell[2]** [ID] **, and A. Ridley[3]**

[1]Physics, Computer Science and Engineering, Christopher Newport University, Newport News, VA, USA, [2]National Institute of Aerospace, Hampton, VA, USA, [3]Climate and Space Sciences and Engineering, University of Michigan, Ann Arbor, MI, USA

Abstract In order to assess the effects of ionospheric feedback on different modes of energy transport in the magnetosphere, we investigate an isolated substorm and a steady magnetospheric convection (SMC) event with very similar solar wind drivers. The primary focus is on a comparison between the isolated substorm and the substorm that initiates the SMC. Auroral data from Polar UVI LBHl and LBHs, along with assimilative mapping of the ionosphere electrojet potential patterns are used as inputs to the global ionosphere-thermosphere model to calculate conductances and Joule heating rates. Results from this study show that the conductances both before and during the events play a large role the ability of the magnetosphere to remain in steady driven state. The substorm that initiates the SMC event shows very different signatures in the ionosphere than isolated substorm; these signatures indicate that there is very weak substorm current wedge, or possibly a pseudo-breakup.

1. Introduction

When the interplanetary magnetic field (IMF) is southward and of moderate strength, energy and particles from the solar wind are loaded in the magnetotail. Eventually, the particles and energy need to be unloaded; this usually happens in the form of an isolated substorm. The term *isolated* indicates that the substorm is a single event and is not part of a larger geomagnetic storm or periodic substorm event. If the driving continues and is fairly steady, the magnetosphere may enter a mode of energy transport where there is no major loading and unloading; rather, the energy is continuously diverted and magnetospheric convection is steady on a large scale. This type of event is referred to as a *steady magnetospheric convection* event or SMC. Most SMCs start after an initiating substorm; however, both Kissinger et al. (2011) and DeJong et al. (2008) found that about 10% of SMC events do not appear to have a preceding, or initiating, substorm. Sergeev et al. (1994) showed that the configuration of the magnetotail during an SMC lies between that of a substorm recovery phase and that of a substorm growth phase. These results indicate that a substorm may be necessary for the magnetosphere to enter into an active steady state such as an SMC. This raises questions about how important initiating substorms are to SMC events and how they differ from isolated substorms.

These two event types can have similar drivers (DeJong et al., 2009; Partamies et al., 2009). While isolated substorms have been studied extensively, SMCs and their initiating substorms have not. Juusola et al. (2013) and DeJong (2014) found that SMCs are more likely to occur during weak or nonstorm times. Kissinger et al. (2010) show that there are many fast flows in the tail during SMCs and that the flows occur along dawn and dusk as opposed to the night side.

Many studies have investigated the solar wind drivers that lead to an active steady state (SMC) as opposed to a loading and unloading state (substorm). While differences are found in the drivers, there are also many times when the driving for these two event types can be very similar (DeJong et al., 2009; Partamies et al., 2009). Thus, drivers alone cannot account for the differences in the magnetospheric dynamics during these events, so we will examine the role ionospheric feedback in determining why the magnetosphere enters these different states. The modeling results of Ridley et al. (2004) show that ionospheric conductance, both seasonal and auroral, can affect the state of the magnetosphere. Raeder et al. (1996) found that specifying a higher conductance in their simulations allows the magnetosphere to remain in a steady state. Along with these findings, more recently, Welling and Liemohn (2016) show that current models do not accurately capture the storm time magnetospheric dynamics when the ionospheric feedback is not included. This is most likely due
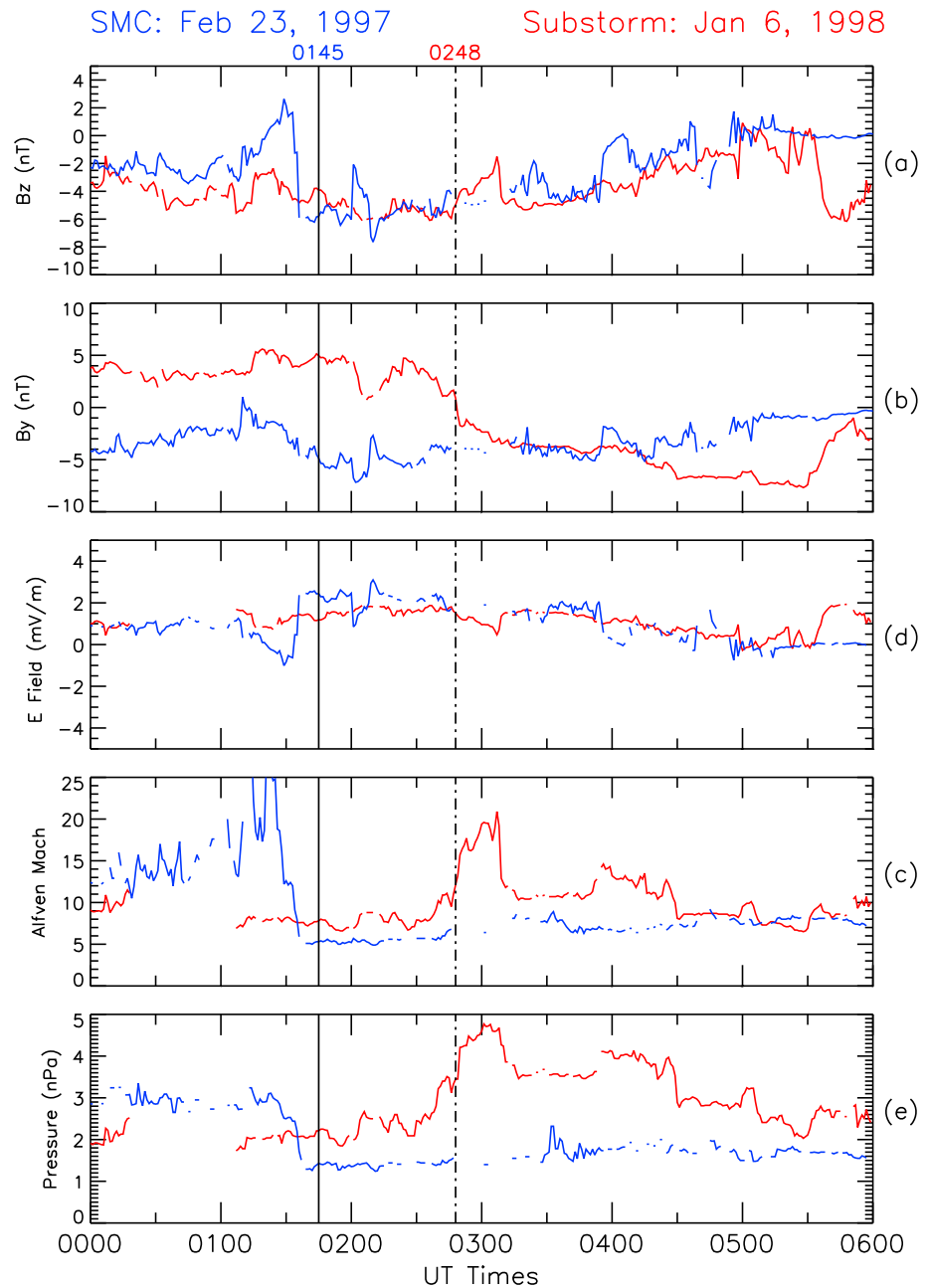
Figure 1. Stack plot of the drivers for the substorm on 6 January 1998 in red and the steady magnetospheric convection (SMC) on 23 February 1997 in blue. The panels from top to bottom are as follows: IMF B_z, IMF B_y, electric field, Alfvenic Mach number, and dynamic pressure. The solid vertical line represents the onset of the substorm that precedes the SMC, and the dotted vertical line is the onset of the isolated substorm.

to the fact that Pederson and Hall conductances in the auroral zone are tied to field aligned currents (Knight et al., 1972).

In order to isolate the effects of the ionosphere on the dynamics of the magnetosphere, we selected two events with very similar drivers. We investigate an isolated substorm that occurred on 6 January 1998 at 0248 UT and an SMC that occurred 23 February 1997 with the onset of the initiating substorm at 0145 UT. Since these two events occur in winter and at a very similar universal time, seasonal differences or magnetometer locations should not affect the results. For the comparison of the ionosphere during these events, we use the global ionosphere-thermosphere model (GITM) to calculate both Pederson and Hall conductances along with Joule heating rates (Ridley et al., 2006). Additionally, we use Polar UVI auroral energy flux, the average auroral
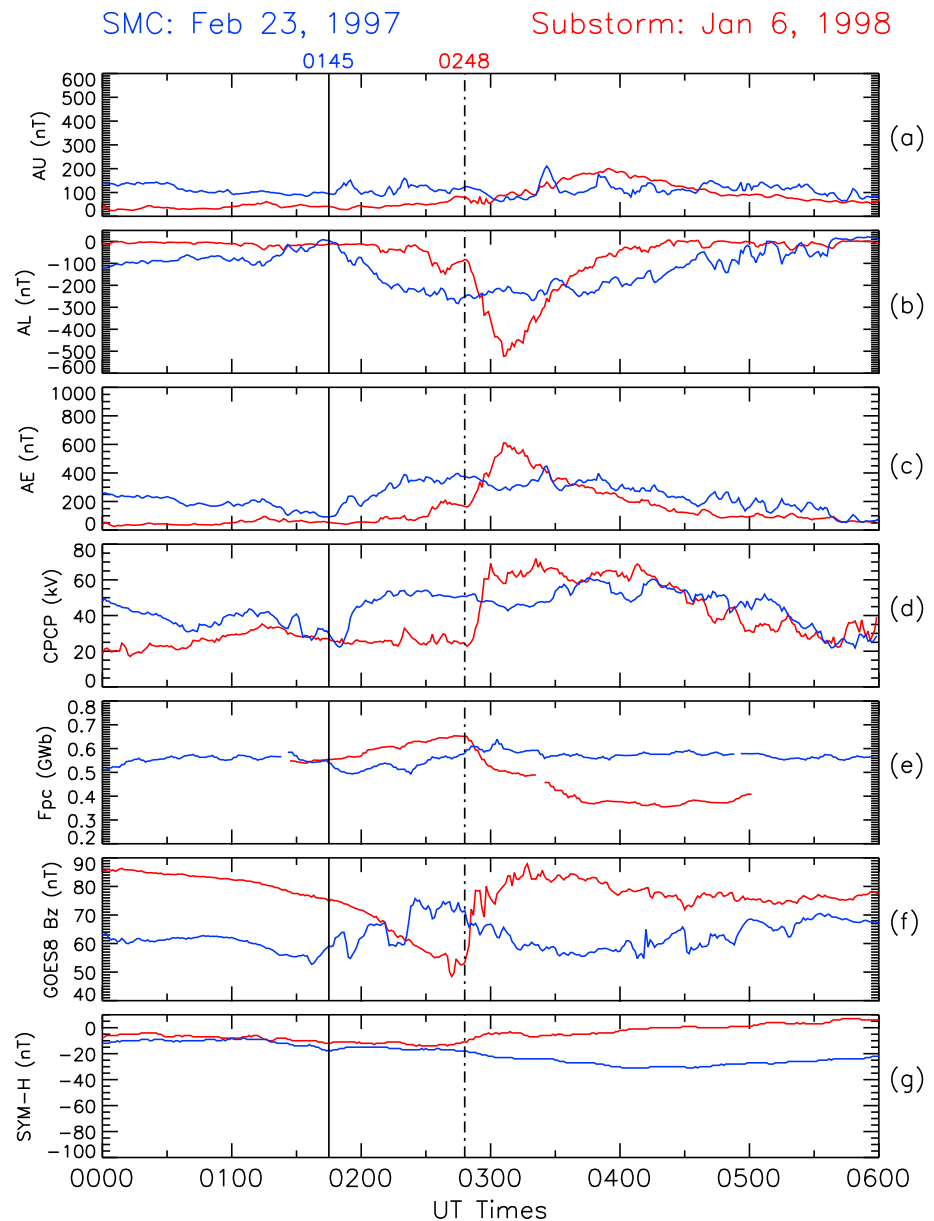
Figure 2. A stack plot of the magnetospheric responses for the substorm on 6 January 1998 in red and the steady magnetospheric convection (SMC) on 23 February 1997 in blue. The panels from top to bottom are as follows: AU, AL, AE, cross polar cap potential, open magnetic flux, GOES 8 B_z, and Sym-H. The solid vertical line represents the onset of the substorm that precedes the SMC, and the dotted vertical line is the onset of the isolated substorm.

energy (Germany et al., 1994), and assimilative mapping of the ionosphere electrojet (AMIE) potential patterns as inputs for the model. Along with the modeling result, we compare the residual ionospheric potential patterns after the onset of the substorms, similar to the study by Cai et al. (2006).

2. Drivers and Indicies

The solar wind drivers and IMF conditions for each event are plotted in Figure 1, where the blue line represents the SMC and the red line the isolated substorm. The solid and dotted vertical lines represent the onset times for the SMC initiating substorm and the isolated substorm respectively. The data for this plot come from the OMNI data set. The IMF B_z (Figure 1a) and the electric field (Figure 1c) are very similar for both events, with the small exception of the increase and drop in B_z about 15 min before the onset of the SMC initiating substorm, indicating a possible tigger for the SMC. IMF B_y remains negative and steady during the SMC, but it changes
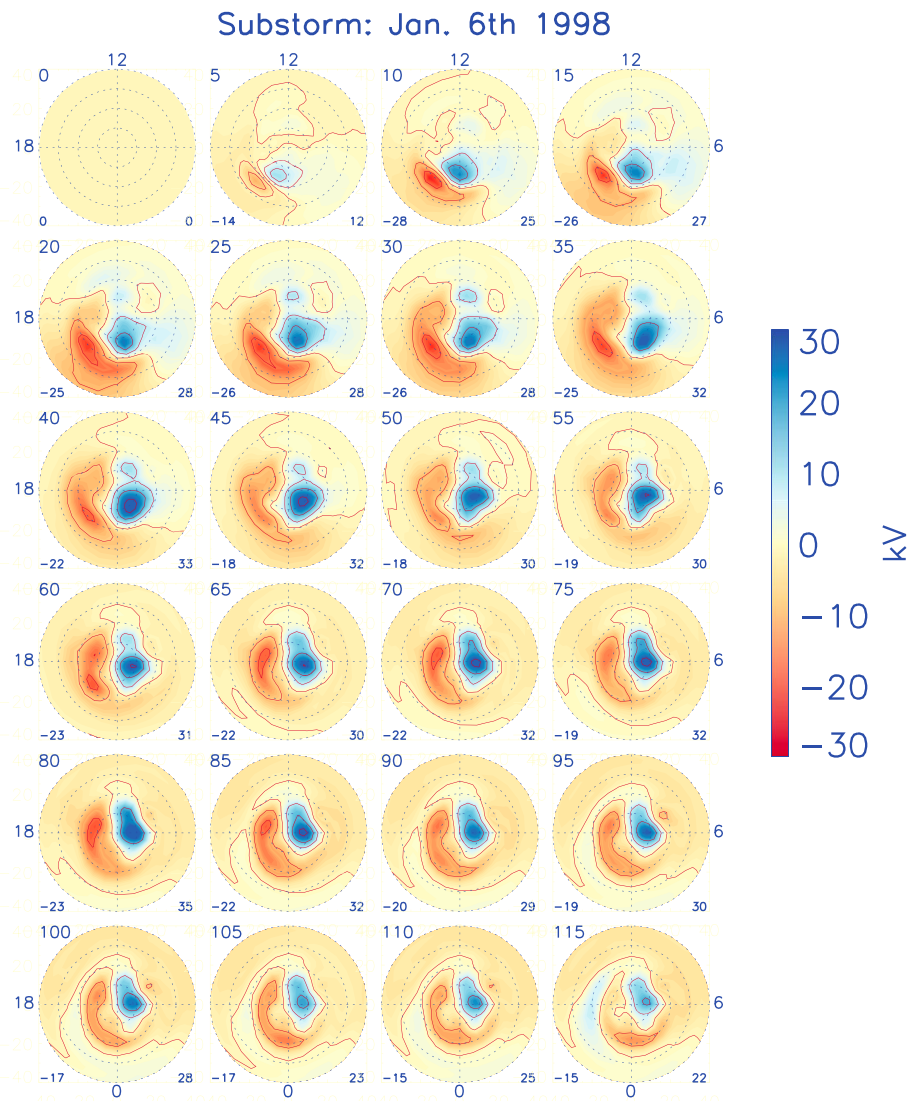
Figure 3. Potential patterns from AMIE, the onset of the substorm (0248) has been removed from all times post onset. Thus, the patterns shown are the residual patterns from the event. AMIE = assimilative mapping of ionospheric electrodynamics.

direction from positive to negative at the onset of the isolated substorm. Both the dynamic pressure and the Alfvenic Mach number drop just before the start of the SMC event, but they increase at the onset of the isolated substorm. These figures indicate that the isolated substorm is most likely triggered by the change in pressure, Mach number, and B_y. Despite these small differences, these two events share very similar drivers and we should expect a similar response in the magnetosphere. However, this is not what occurs.

Figure 2 shows the magnetospheric response to these similar drivers; AU, AL, AE, and Sym-H are all from the OMNI data set. The F_{PC}, or open magnetic flux, was calculated for DeJong et al. (2007) and is once again plotted here to show the approximate change in the polar cap. The cross polar cap potential or CPCP is calculated from AMIE (Kihn & Ridley, 2005). The B_z component of the magnetic field from the GOES 8 satellite in GSM coordinate is also plotted. During this time GOES 8 was on the nightside in the premidnight sector when both substorms occurred. The AU and the Sym-H show very little activity for both events. The Sym-H is close to zero for the isolated substorm, and it only decreases to about −30 nT for the SMC. Thus, neither of these events occur during storm time. While the IMF B_z and the electric fields are very similar for these events (Figure 1), their AL response is very different (Figure 2b). At the onset of the SMC initiating substorm (solid line) there is a decrease in AL from 0 nT to about −300 nT over an hour, indicating a weak substorm that then leads into
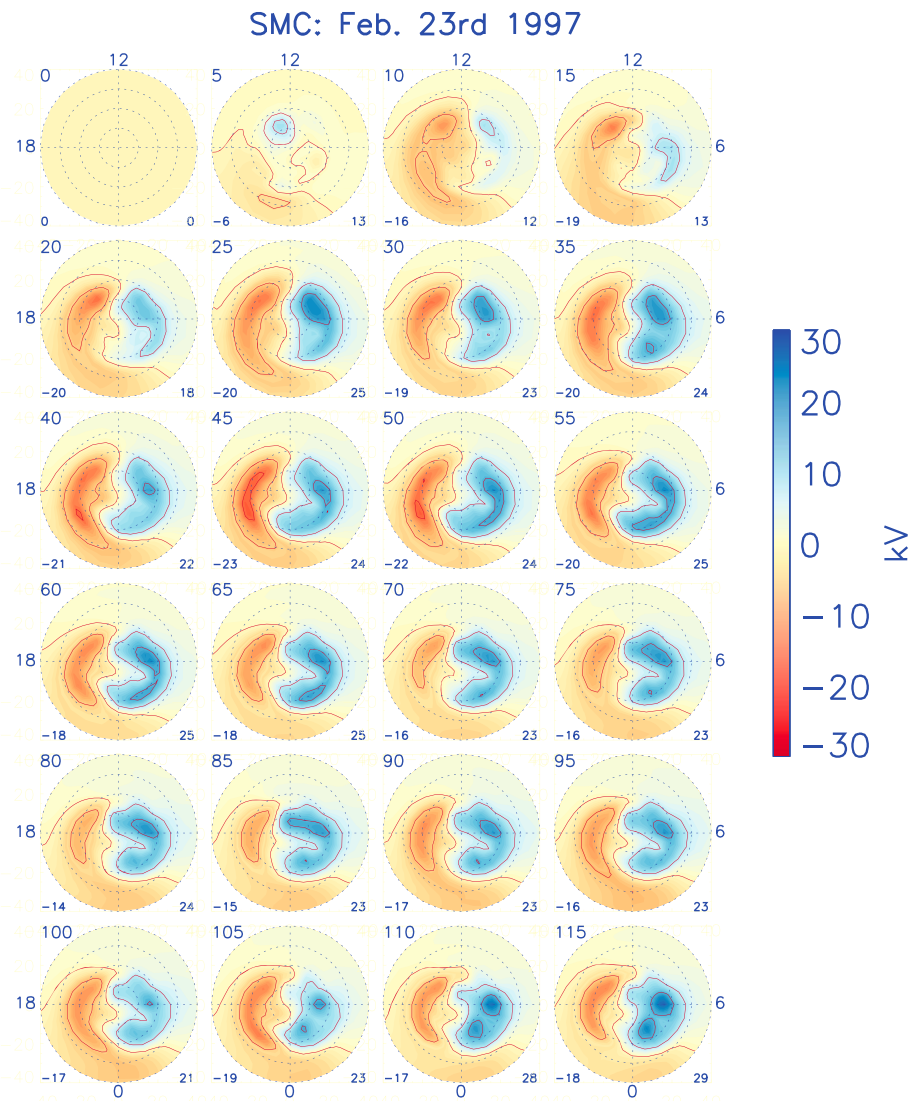
Figure 4. Potential patterns from AMIE, the onset of the SMC (0145) has been removed from all times post onset. Thus, the patterns shown are the residual patterns from the event. AMIE = assimilative mapping of ionospheric electrodynamics; SMC = steady magnetospheric convection.

the SMC. This is also roughly the time of the CPCP increase, confirming an onset time. The GOES B_z shows a positive change during this time, possibly indicating that a dipolarization event occurred. This SMC was identified using the method in DeJong and Clauer (2005), which requires a steady F_{PC} for at least 3 hr, and this can be seen in Figure 2e. The onset of the isolated substorm is much more obvious in AL, the CPCP, and the F_{PC} as all changes line up with the onset time of 0248 UT (dotted line). The AL drops to about −500 nT 20 min after the onset, which is then followed by a recovery phase that lasts about 1 hr. At the same time, the polar cap potential difference changes from 20 to 70 kV and the polar cap flux shrinks from 0.65 to 0.35 GWb. The GOES B_z drops from almost 90 nT down about 50 nT before the onset as the magnetic fields at geosynchronous orbit are stretched, then a rapid increase at the substorm onset indicates the dipolarization that occurs at the onset of the expansion phase.

The precondition for these two events can be seen from the 0000 UT point on both days. While the IMF B_z is negative and moderate (−3 nT) the magnetosphere shows little to no response on 6 January 1998 with AL very close to zero until the onset of the substorm. During the same IMF B_z conditions, the magnetosphere has a response of about −100 nT in AL before the SMC; the AL then quiets down before the onset of the SMC. The differences the magnetsopheric response during the time leading up to these events could very well have an impact on the final response mode of the magnetosphere.
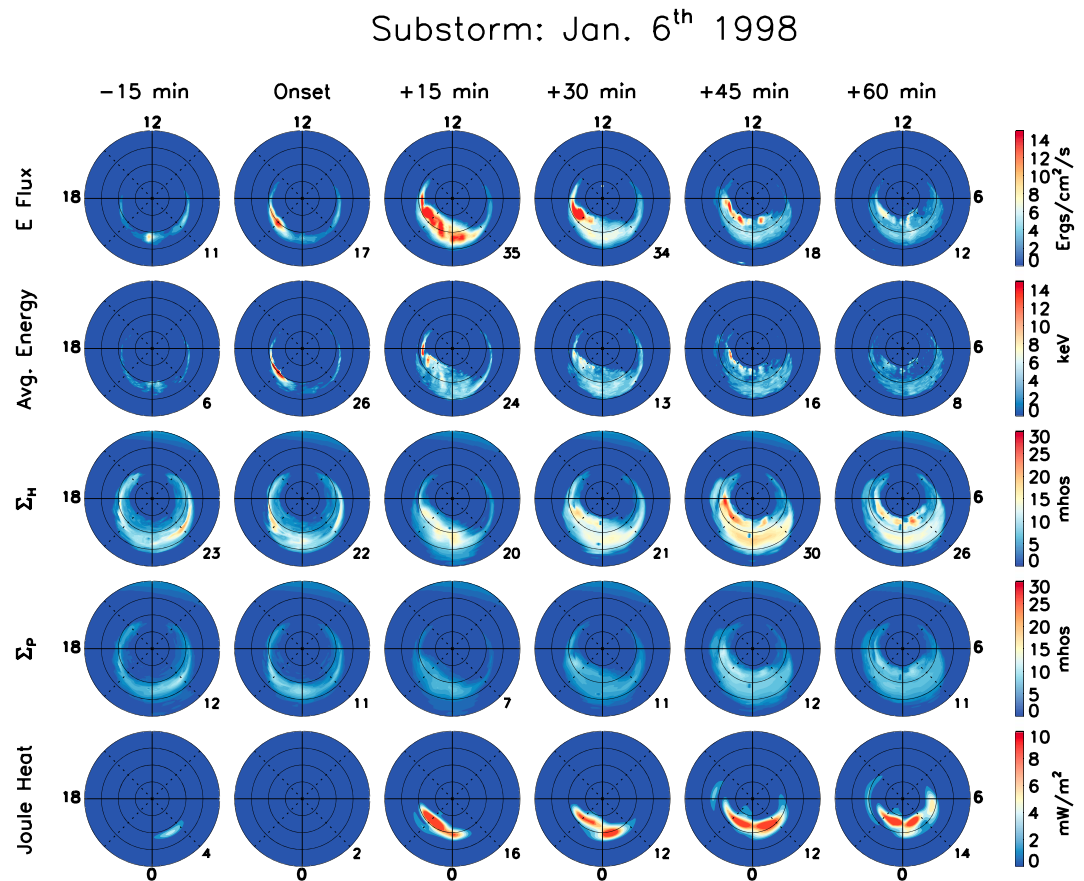
Figure 5. All plots are in MLT coordinates with noon at the top and midnight at the bottom. The first column is 15 min before the onset of the isolated substorm, the second is at the onset time (0248 UT), and the next four columns are in 15-min increments after the onset up to 1 hr. MLT = magnetic local time.

3. Modeling and Methods

We utilize the GITM to simulate auroral conductances and Joule heating (Ridley et al., 2006). In order to simulate the state of the ionosphere-thermosphere during the SMC and the isolated substorm events, we input the solar wind drivers, the AMIE potential patterns, the calculated average auroral energy (Germany et al., 1994), and the auroral energy flux from Polar UVI. The auroral energy flux is taken the from the Polar UVI LBHl filter, and the average auroral energy is calculated from the UVI images using the ratio of the measured LBHl to the measured LBHs and the atmospheric model of Germany et al. (1994). Because the LBHl and LBHs images are not taken at the same time, as UVI switches through the filters, the images must be linearly interpolated to match the time stamp of the other image. This allows us to generate an average energy and energy flux input approximately every 1 to 2 min. These time-dependent auroral drivers are then input into GITM as the simulation evolves, allowing us to investigate how the ionosphere responds to these time-varying high latitude inputs.

We employ GITM, because it is the only coupled ionosphere-thermosphere model to relax the hydrostatic constraint, which allows it to self-consistently solve the momentum equation in the vertical direction (Ridley et al., 2006). This allows GITM to accurately simulate the ionospheric response to intense, localized heating in the aurora (Deng, Richmond, et al., 2008). GITM also includes ionospheric chemistry coupled with neutral chemistry, self-consistently. Moreover the ionization and dissociation related to auroral precipitation are included as part of the chemical drivers. This allows us to calculate the net ionization in the ionosphere during these events, which further allows us to calculate the Pedersen and Hall conductivities in the ionosphere according to the well-known formulas involving the ion-neutral collision frequencies and the local ion gyrofrequency (Schunk & Nagy, 2004). GITM also accounts for both Joule heating and direct heating by auroral precipitation, allowing us to combine thermal structure, dynamical, and chemical responses of the upper atmosphere
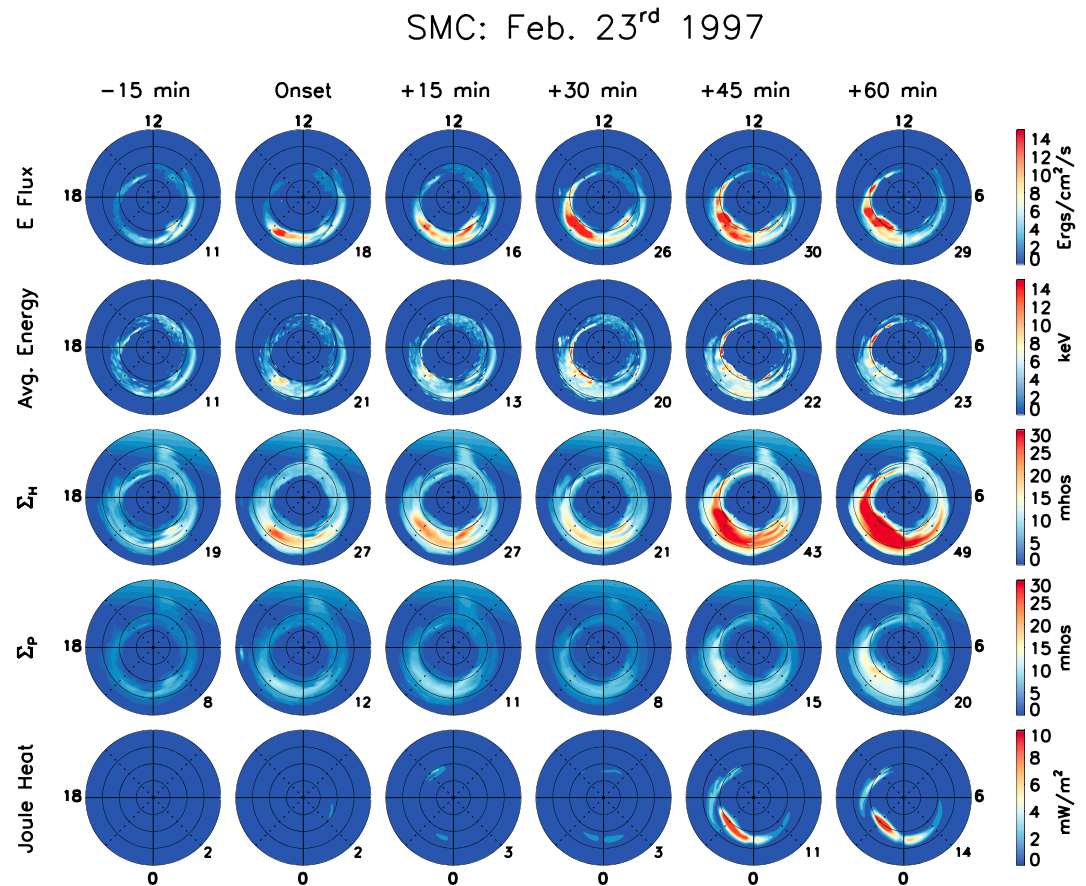
Figure 6. All plots are in MLT coordinates with noon at the top and midnight at the bottom. The first column is 15 min before the onset of the initiating substorm, the second is at the onset time (0145 UT), and the next four columns are in 15-min increments after the onset up to 1 hr. MLT = magnetic local time.

to the high-latitude driving specified by AMIE and Polar UVI. We use the model-simulated conductances to examine the state of the ionosphere during the SMC and the isolated substorm.

Each GITM simulation was run for an initial 24 hr to remove any impacts from startup. We include date-appropriate F10.7-cm values, the waves and tides provided by the global scale wave model (Hagan et al., 1999), and lower boundary temperatures and winds are provided by the NRL MSIS-00 (Picone et al., 2002). The AMIE potential patterns were incorporated into GITM at each time step to drive the upper atmosphere through an imposed magnetospheric electric field and through particle precipitation into the auroral zones. We column-integrate the conductances and the joule heating rates within GITM itself during run time to ensure the self-consistency of the outputs. These methods are consistent with numerous studies of the thermosphere-ionosphere (Bell et al., 2014; Bougher et al., 2015; Deng, Maute, et al., 2008; Riley et al., 2006).

4. Results

The potential patterns for the isolated substorm and the SMC are created from the AMIE with inputs of only magnetometers as in Ridley et al. (2004) and Cai et al. (2006). The focus of this study is the development of the DP1 pattern during the expansion phase of the isolated substorm and the substorm preceding the SMC. The DP1 pattern is associated with the substorm current wedge, and it begins to develop right after the onset of the expansion phase and continues to strengthen during this phase. A similar pattern was found for global sawtooth injections, with a larger potential difference than the substorms (Cai et al., 2006). During the substorm expansion phase, the DP1 potential pattern dominates, but it can be difficult to observe. Thus, to isolate the pattern that arises during the events, the onset time must first be removed from all succeeding times (Cai et al., 2006), creating a residual pattern.
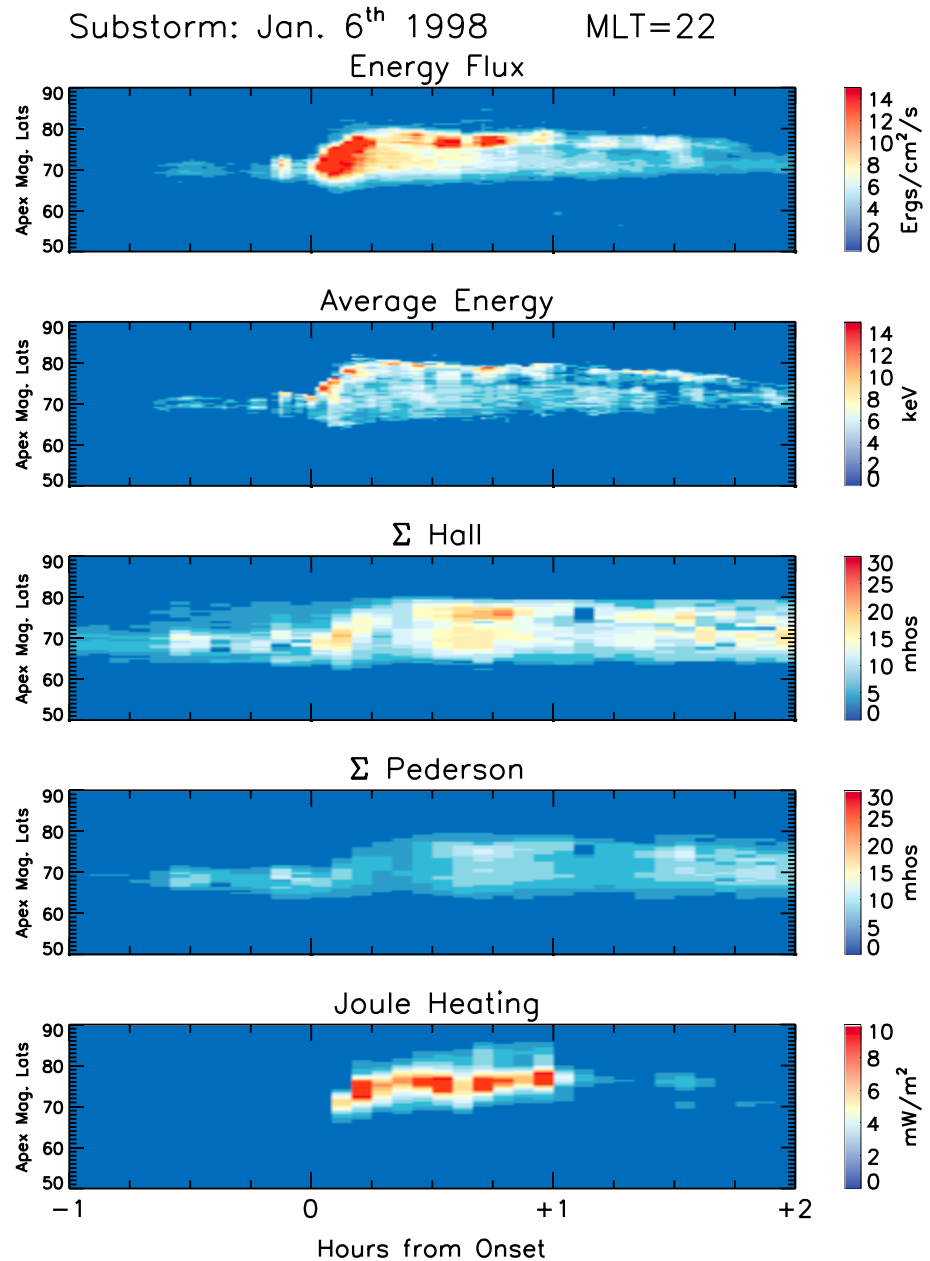
Figure 7. Keograms from an MLT of 22, with the same data from Figure 5 starting from 1 hr before onset to 2 hr after the onset. MLT = magnetic local time.

Figure 3 shows the AMIE potential patterns for the isolated substorm on 8 January 1998. The plots are in magnetic local time (MLT) coordinates with noon at the top, and each dotted circle is 10° magnetic latitude. All of the plots have had the onset of the expansion phase, 0248 UT, removed, leaving the first plot blank after the subtraction. The plots that follow are snapshots at 5-min intervals for the 2 hr after the start of the isolated substorm. The DP1 pattern begins to appear as early as 5 min after the onset, with a peak in the pattern at 40 min, as seen by the blue contours. By minute 60, the pattern has changed back to an enhanced DP2 pattern during the substorm's recovery phase. After 2 hr the potential patterns have weakened to their initial levels. These results are consistent with those shown for isolated substorms and global sawtooth oscillations by Cai et al. (2006).

The initiating substorm of the SMC shows very different residual potential patterns than those of the isolated substorm. Figure 4 shows the SMC initiating substorm on 23 February 1997, in the same format as Figure 3.
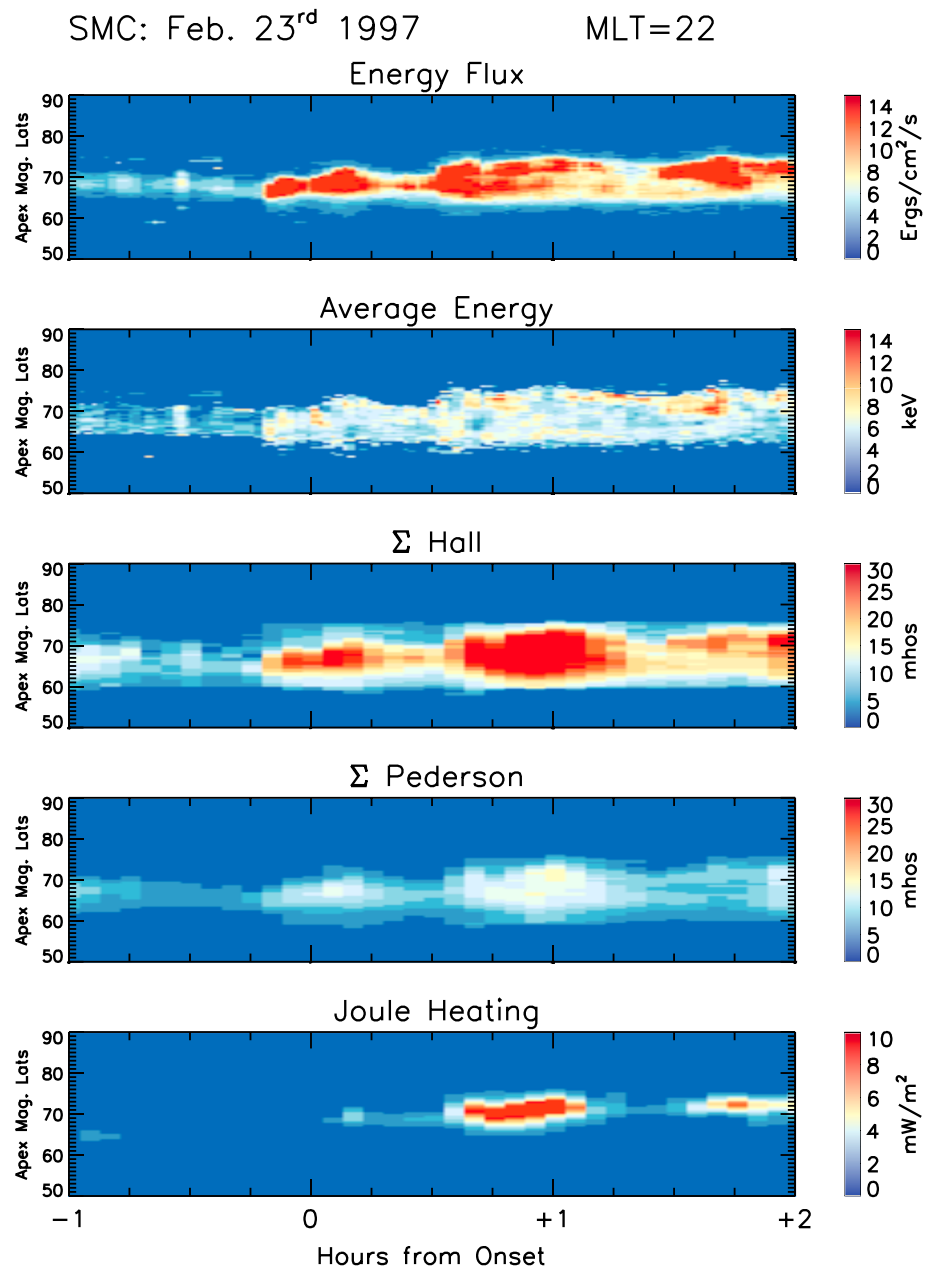
Figure 8. Keograms from an MLT of 22, with the same data from Figure 6 starting from 1 hr before onset to 2 hr after the onset. MLT = magnetic local time.

The residual potential patterns show an enhanced two-cell convection, DP2, with no sign of a DP1 pattern. Since there is a substorm before the magnetosphere enters the steady state, a DP1 pattern is to be expected. There is a small positive cell that develops around 30 min after the onset, and this could reveal a very weak DP1 pattern overlapping the DP2. However, when the 0215 UT pattern (30 min after onset) was removed as the background, there was no indication of a DP1 pattern. This lack of a DP1 pattern shows that the substorms that precede SMCs may in fact be different than isolated substorms.

Figures 5 and 6 are MLT plots of the auroral energy flux, average auroral energy, integrated Hall conductance, integrated Pederson conductance, and Joule heating for the isolated substorm and the SMC initiating substorm, respectively. The auroral energy fluxes are from Polar UVI LBHl images, the average auroral energy is calculated from Germany et al. (1994), and the conductances and Joule heating are calculated from GITM. The first column of images are from 15 min before the onset of the expansion phase and each succeeding

column snapshots at 15-min increments up to 1 hr after the onset. The plots have magnetic north at the center of the image, and the circles represent 10° magnetic latitude down to 50°. The top of each circle is magnetic local noon, and the bottom is magnetic local midnight, and the sides are dawn and dusk. The number on the bottom right of each plot is the maximum value at that time stamp. As expected, the integrated Hall conductances are higher than the Pederson conductances for both the isolated substorm and the initiating substorm of the SMC. Both patterns follow the auroral images (top row) fairly closely. The same data are shown in Figures 7 and 8 in keogram format for 22 MLT; this MLT was chosen since both onsets occur near this location. The data and color bars for each row are the same for all four figures. The keograms begin 1 hr before onset and continue to 2 hr after onset.

The isolated substorm on 6 January 1998 in Figures 5 and 7 proceeds as anticipated in the auroral images. The substorm enters into the recovery phase about 1 hr after the onset, even though the solar wind B_z is still slowly approaching zero and will not become positive for another hour (Figure 1a). The Joule heating begins about 5 min after onset and ends when once the recovery phase begins. Palmroth et al. (2004) found that Joule heating increases about 5 min after a pressure pulse during steady IMF conditions. Thus, the Joule heating is most likely a combination of the onset of the substorm and the pressure pulse seen in Figure 1. The Hall conductance continues to increase even as the auroral energy flux starts to diminish. By the end of the time frame in Figure 7, the substorm has ended and the aurora is back to presubstorm levels.

The SMC and its initiating substorm on 23 February is shown in Figures 6 and 8. The auroral energy flux during the SMC does not change significantly, and the initiating substorm does not show a strong poleward movement, as seen in both Figure 6 and the F_{PC} in Figure 2. The auroral energy flux and conductances do intensify and spread toward dawn and dusk, as seen in Figure 6. The Joule heating does not increase significantly until 40 min after the onset of the initiating substorm. We note in Figure 8 that the aurora becomes active about 10 min before the onset on the substorm, which could be due to a preonset pseudo-breakup. However, this brightening is not considered the onset time as it does not occur at the same time as decrease in AL and the increase in CPCP (Figure 2). The SMC event continues past the time frame shown in Figure 8. By definition from DeJong and Clauer (2005), the event must last at least one more hour for a total of 3 hr to be classified as an SMC.

5. Discussion

The results in the previous sections show that these two events types can have distinct ionospheric signatures. However, one of the most significant differences is the preconditioning before the SMC event. Not only can it be seen in the AL and AE data but also in the keograms in Figures 7 and 8 that show the aurora and integrated conductances are more active before the onset of the SMC. It is unusual that the solar wind IMF B_z, which is at −4 nT for 3 hr, does appear to impact the magnetosphere and ionosphere before the isolated substorm. The interval before the SMC on the other hand has activity that most likely leads to preconditioning of the ionosphere and magnetosphere allowing the SMC to occur. The higher conductance before the SMC event most likely plays a role in allowing the magnetosphere to unload energy in smaller amounts such as fast flow rather than one large unloading. If the conductance is lower, then the energy cannot flow as well, forcing the magnetotail to store the energy until the system is overloaded and the energy is unloaded all at once.

During the events there are also differences in the ionosphere both the integrated Pederson and Hall conductances are higher during the SMC; however, it takes longer for these conductances to build up during this event. For the SMC initiating substorm, the peaks in the conductances occur an hour after onset and they remain strong for the duration of the time shown. The peaks are also much more spread out in the auroral zone during this event, with the largest Hall conductances at 49 mhos and the Pederson at 20 mhos, as seen in Figure 6. By contrast, the peak conductances for the isolated substorm occur approximately 45 min after the onset, with the Hall at 37 mhos and Pederson at 12 mhos. The auroral energy flux and average energy however peak at the onset of the isolated substorm. Thus, the auroral conductance is much higher when the magnetosphere is in a steady state. This agrees with Raeder et al. (1996) who found that higher conductances in MHD simulations lead to a steadier magnetosphere. This suggests that higher conductance allow the magnetosphere to slowly and steadily unload its energy as opposed to having a large reconfiguration event like a strong substorm.

Another interesting observation is that neither AL nor the solar wind parameters during these events are well correlated with the Hall conductance as found by Aksnes et al. (2002). There is a small amount of activity in AL before the onset of both events (Figure 2b), but during the SMC it slowly decreases over the first hour and never gets below −300 nT. On the other hand, the isolated substorm AL decreases sharply over the first 30 min and extends beyond −500 nT before entering the recovery phase. The solar wind conditions are almost exactly the same for these two events, yet the Hall conductance is quite different. Thus, if either AL or the solar word is related to the Hall conductance, then it is not apparent in our results, since the event with the weaker AL has a much stronger Hall conductance.

The Joule heating rates for these events do not show the same patterns as the conductances. Both events reach a maximum heating rate of close to 15 mW/m^2. During the isolated substorm the heating starts almost immediately after the onset, whereas the heating during the SMC does not initiate until 40 min into the event. The Joule heating also takes place a much higher latitude (70°–80°) during the isolated substorm than during the SMC (60°–70°). Bjoland et al. (2015) found enhancements in the Joule heating at 70° latitude at 15 MLT and 2 MLT during all IMF conditions. We only see the dayside (15 MLT) enhancement during the SMC starting at 15 min after onset, Figure 6. We also have a slight increase in Joule heating that occurs at 2 MLT at 15 min before the onset of the isolated substorm and 45 min after the onset in Figure 5. Most of the simulated Joule heating during these events occur around at dusk, where the auroral inputs are the most intense.

Zhou et al. (2011) showed that nightside enhancements in Joule heating during substorms is associated with unloading, or a substorm current wedge. Thus, the isolated substorm shows a strong current wedge signature in both the Joule heating (Figure 5) and the potential patterns (Figure 3). These potential patterns during the isolated substorm will produce a strong electric field that subsequently induces stronger ion velocities. These enhanced ion winds, since they are flowing against the background neutral winds, naturally produce stronger Joule heating in those regions.

The lack of a DP1 pattern during the SMC initiating substorm along with the weak substorm signatures seen in the GOES8 data and auroral indices indicates the initiating substorm of the SMC is very weak or even a pseudo-breakup. Thus, while a substorm current wedge is intitially created the energy from tail soon gets diverted through enhanced convection allowing the magnetosphere to enter a steady state. This is consistent with the auroral images shown in Figure 6 and the F_{PC} in Figure 2, where the aurora does not show a large poleward movement but rather spreads out along the oval. Kissinger et al. (2010) showed that fast flows, carrying energy from the magnetosphere to the ionosphere, occur frequently during SMCs. If these flows can carry enough energy then a substorm current wedge, or at least not a strong one, may not need to fully develop during these substorms that initiate SMCs. This indicates that the magnetosphere does not have a strong tail reconfiguration during the expansion phase of the SMC initiating substorm.

The Joule heating also supports the idea that there is only a weak substorm current wedge, or unloading, associated with the onset of the substorm that initiates the SMC. The Joule heating does not increase until 35 min into the event (Figures 6 and 8), about the same time a small positive cell appears to overlap with the enhanced convection pattern of the SMC (Figure 4). This could indicate that a weak current wedge is established during the SMC.

Liou et al. (2011) also studied this substorm but identified the 0215 UT auroral brightening as the substorm onset instead of our 0145 UT onset. However, since there is no real change in AL, CPCP, or F_{CP} at this time, it is more likely just an enhancement in activity. Thus, the SMC starts off without a current wedge but enhances the aurora and AL by unloading in small amounts as opposed to one large reconfiguration.

Overall, the initiating substorm of this SMC is very different from an isolated substorm. In order to more fully investigate whether a weak substorm current wedge is normal for initiating substorms of SMC and if most SMCs have a higher conductance, more events must be studied.

This study has shown that there are more questions to investigate:

1. How similar are other SMC initiating substorms to this one, including preconditioning?
2. How important is the larger Hall conductance in allowing the magnetosphere to remain steady? Does the higher conductivity allow the magnetosphere to stay steady or are the small fast flows creating a higher conductance?

6. Summary

The ionosphere during two substorms with very similar solar wind drivers are investigated in this study, one substorm is isolated while the other initiates a SMC event. Both events occur during a similar universal time so that our differences in the data are not due to instrument location and both take place during the winter months to help account for any difference in the conductivity of the ionosphere. We found that the ionosphere plays a large role in these two events, allowing one to remain in an enhanced steady state, while the other unloads the magnetosphere and goes back to a quiet state. The major findings are listed below.

1. Preconditioning appears to play a large role in the type of event the magnetosphere enters.
2. There is no DP1 current development after the onset of the SMC initiating substorm; instead, there is an enhanced DP2 convection pattern.
3. Integrated Hall conductance is much greater during the SMC initiating substorm and continues to increase throughout the SMC.
4. Joule heating is stronger during the isolated substorm, and there is little to no Joule heating until 30 min into the SMC.
5. The weaker substorm or pseudo-breakup that initiates SMC is weak enough that the energy from the magnetosphere can quickly be deposited by smaller fast flows that reach the ionosphere.

References

Aksnes, A., Stadsnes, J., Bjordal, J., Østgaard, N., Vondrak, R. R., Detrick, D. L., et al. (2002). Instantaneous ionospheric global conductance maps during an isolated substorm. *Annales Geophysicae*, *20*, 1181–1191. https://doi.org/10.5194/angeo-20-1181-2002

Bell, J. M., Hunter Waite, J., Westlake, J. H., Bougher, S. W., Ridley, A. J., Perryman, R., & Mandt, K. (2014). Developing a self-consistent description of Titan's upper atmosphere without hydrodynamic escape. *Journal of Geophysical Research: Space Physics*, *119*, 4957–4972. https://doi.org/10.1002/2014JA019781

Bjoland, L. M., Chen, X., Jin, Y., Reimer, A. S., Skjæveland, Å., Wessel, M. R., et al. (2015). Interplanetary magnetic field and solar cycle dependence of Northern Hemisphere F region joule heating. *Journal of Geophysical Research: Space Physics*, *120*, 1478–1487. https://doi.org/10.1002/2014JA020586

Bougher, S. W., Pawlowski, D., Bell, J. M., Nelli, S., McDunn, T., Murphy, J. R., et al. (2015). Mars global ionosphere-thermosphere model: Solar cycle, seasonal, and diurnal variations of the Mars upper atmosphere. *Journal of Geophysical Research: Planets*, *120*, 311–342. https://doi.org/10.1002/2014JE004715

Cai, X., Clauer, C., & Ridley, A. (2006). Statistical analysis of ionospheric potential patterns for isolated substorms and sawtooth events. *Annales Geophysicae*, *24*, 1977–1991.

DeJong, A. D. (2014). Steady magnetospheric convection events: How much does steadiness matter? *Journal of Geophysical Research: Space Physics*, *119*, 4389–4399. https://doi.org/10.1002/2013JA019220

DeJong, A. D., Cai, X., Clauer, C. R., & Spann, J. F. (2007). Aurora and open magnetic flux during isolated substorms, sawteeth, and SMC events. *Annales Geophysicae*, *25*, 1865–1876. https://doi.org/10.5194/angeo-25-1865-2007

DeJong, A. D., & Clauer, R. C. (2005). Polar uvi images to study steady magnetospheric convection events: Initial results. *Geophysical Research Letters*, *32*, L24101. https://doi.org/10.1029/2005GL024498

DeJong, A. D., Ridley, A. J., Cai, X., & Clauer, C. R. (2009). A statistical study of BRIs (SMCs), isolated substorms, and individual sawtooth injections. *Journal of Geophysical Research*, *114*, A08215. https://doi.org/10.1029/2008JA013870

DeJong, A. D., Ridley, A. J., & Clauer, C. R. (2008). Balanced reconnection intervals: Four case studies. *Annales Geophysicae*, *26*, 3897–3912. https://doi.org/10.5194/angeo-26-3897-2008

Deng, Y., Maute, A., Richmond, A. D., & Roble, R. G. (2008). Analysis of thermospheric response to magnetospheric inputs. *Journal of Geophysical Research*, *113*, A04301. https://doi.org/10.1029/2007JA012840

Deng, Y., Richmond, A. D., Ridley, A. J., & Liu, H.-L. (2008). Assessment of the non-hydrostatic effect on the upper atmosphere using a general circulation model (GCM). *Geophysical Research Letters*, *35*, L01104. https://doi.org/10.1029/2007GL032182

Germany, G., Torr, D. G., Richards, P. G., Torr, M. R., & Jong, S. (1994). Determination of ionospheric conductivities from FUV auroral emission. *Journal of Geophysical Research*, *99*(A12), 23,297–23,305.

Hagan, M. E., Burrage, M. D., Forbes, J. M., Hackney, J., Randel, W. J., & Zhang, X. (1999). GSWM-98: Results for migrating solar tides. *Journal of Geophysical Research*, *104*(A4), 6813–6828. https://doi.org/10.1029/1998JA900125

Juusola, L., Partamies, N., & Tanskanen, E. (2013). Effect of the ring current on preconditioning the magnetosphere for steady magnetospheric convection. *Geophysical Research Letters*, *40*, 1917–1921. https://doi.org/10.1002/grl.50405

Kihn, E. A., & Ridley, A. J. (2005). A statistical analysis of the assimilative mapping of ionospheric electrodynamics auroral specification. *Journal of Geophysical Research*, *110*, A07305. https://doi.org/10.1029/2003JA010371

Kissinger, J., Hsu, T.-S., & Angelopoulos, V. (2011). Steady magnetospheric convection and stream interfaces: Relationship over a solar cycle. *Journal of Geophysical Research*, *116*, A00I19. https://doi.org/10.1029/2010JA015763

Kissinger, J., McPherron, R. L., Angelopoulos, V., Hsu, T.-S., & McFadden, J. P. (2010). An investigation of the association between steady magnetospheric convection and CIR stream interfaces. *Geophysical Research Letters*, *37*, L04105. https://doi.org/10.1029/2009GL041541

Knight, D. E., Uribe, R., & Woodgate, B. E. (1972). Extreme ultra-violet absorption cross-sections in the Earth's upper atmosphere. *Planetary and Space Science*, *20*, 161–164. https://doi.org/10.1016/0032-0633(72) 90098-0

Liou, K., Zhang, Y.-L., Newell, P. T., Paxton, L. J., & Carbary, J. F. (2011). TIMED/GUVI observation of solar illumination effect on auroral energy deposition. *Journal of Geophysical Research*, *116*, A09305. https://doi.org/10.1029/2010JA016402

Palmroth, M., Pulkkinen, T. I., Janhunen, P., McComas, D. J., Smith, C. W., & Koskinen, H. E. J. (2004). Role of solar wind dynamic pressure in driving ionospheric Joule heating. *Journal of Geophysical Research*, *109*, A11302. https://doi.org/10.1029/2004JA010529

Partamies, N., Pulkkinen, T. I., McPherron, R. L., McWilliams, K., Bryant, C. R., Tanskanen, E., et al. (2009). Statistical survey on sawtooth events, SMCs and isolated substorms. *Advances in Space Research*, *44*, 376–384. https://doi.org/10.1016/j.asr.2009.03.013

Picone, J. M., Hedin, A. E., Drob, D. P., & Aikin, A. C. (2002). NRLMSISE-00 empirical model of the atmosphere: Statistical comparisons and scientific issues. *Journal of Geophysical Research*, *107*(A12), 1468. https://doi.org/10.1029/2002JA009430

Raeder, J., Berchem, J., & Ashour-Abdalla, M. (1996). The importance of small scale processes in global MHD simulations: Some numerical experiments. In T. Chang & J. R. Jasperse (Eds.), *The physics of space plasmas* (Vol. 14, 403 pp.). Cambridge, MA: MIT Center for Theoretical Geo/Cosmo Plasma Physics.

Ridley, A. J., Deng, Y., & Tóth, G. (2006). The global ionosphere thermosphere model. *Journal of Atmospheric and Solar-Terrestrial Physics*, *68*, 839–864. https://doi.org/10.1016/j.jastp.2006.01.008

Ridley, A., Gombosi, T., & Dezeeuw, D. (2004). Ionospheric control of the magnetosphere: conductance. *Annales Geophysicae*, *22*, 567–584. https://doi.org/10.5194/angeo-22-567-2004

Schunk, R. W., & Nagy, A. F. (2004). *Ionospheres* (570 pp.). Cambridge, MA: Cambridge University Press.

Sergeev, V. A., Pulkkinen, T. I., Pellinen, T. I., & Tsyganenko, N. A. (1994). Hybird state of the tail mangetic configuration during steady convection events. *Journal of Geophysical Research*, *99*(A12), 23,571–23,582. https://doi.org/10.1029/94JA01980

Welling, D. T., & Liemohn, M. W. (2016). The ionospheric source of magnetospheric plasma is not a black box input for global models. *Journal of Geophysical Research: Space Physics*, *121*, 5559–5565. https://doi.org/10.1002/2016JA022646

Zhou, X.-Y., Sun, W., Ridley, A. J., & Mende, S. B. (2011). Joule heating associated with auroral electrojets during magnetospheric substorms. *Journal of Geophysical Research*, *116*, A00I28. https://doi.org/10.1029/2010JA015804